Cement and Concrete Composites 139 (2023) 105051

Contents lists available at ScienceDirect

Cement and Concrete Composites

journal homepage: www.elsevier.com/locate/cemconcomp

Engineered cementitious composites (ECC) with a high volume of volcanic ash: Rheological, mechanical, and micro performance

He Zhu [a], Wei-Hsiu Hu [a], Mohammed Mehthel [b], Thibault Villette [b], Oscar Salazar Vidal [b], Waleed N. Nasser [b], Victor C. Li [a,*]

[a] Department of Civil and Environmental Engineering, University of Michigan, Ann Arbor, MI, 48109, USA
[b] Saudi Aramco, Dhahran, 31311, Saudi arabia

ARTICLE INFO

Keywords:
Engineered cementitious composites (ECC)
Volcanic ash
Local material
Fly ash
Self-healing
Ductile

ABSTRACT

Environmental and economic concerns impel construction materials to employ as many local supplementary cementitious materials as feasible. In this research, a durable Engineered Cementitious Composites (ECC) is developed with the total substitution of fly ash (FA) by volcanic ash (VA). The rheological, mechanical, and micro performance of VA ECC reinforced with polyethylene fibers were comprehensively investigated. Specifically, the severe segregation of VA paste was overcome by systematic engineering of the paste rheology. A minimum paste viscosity of 6 Pa s was found to be effective for fiber dispersion. The compromised compressive strength of VA ECC due to the larger particle size and less pozzolanic activity (compared to FA) was successfully counteracted by the addition of silica fume and the reduction of water to binder ratio. The strain-hardening VA ECC attained 6.7–12.5% of tensile ductility with 46–91 μm of crack width. Moreover, robust self-healing capacity with crack sealing and strength enhancement was demonstrated. The durable ECC holds promise for new constructions and repair of aging infrastructures.

1. Introduction

Concrete is one of the most widely used construction materials because of the advantages of raw constituent wide availability, relatively low cost, and good compressive performance. However, due to the brittle nature of concrete, its tensile strength/strain capacity is significantly lower than compressive strength/strain capacity. Hence, concrete is prone to cracking, which can be caused by external loading or restrained deformation [1,2]. The cracked concrete jeopardizes the structure's durability and safety which results in needed repeated repairs. Therefore, tensile fracture represents a bottleneck to the sustainability of concrete structures.

Engineered cementitious composites (ECC) is a specifically designed fiber-reinforced concrete, which attains high tensile ductility (>3%) by multiple microcracking (usually below 100 μm) [3] beyond the elastic limit. Moreover, tiny cracks can be autogenous healed under water, water-dry, $Ca(OH)_2$, and Na_2SO_4 environments [4–8]. Owing to the superior tensile performance, ECC has been successfully applied in infrastructure construction and repair, such as slabs, bridges, dams, buildings, and pipelines [3,9,10]. However, coarse aggregates are eliminated in ECC compositions as required by micromechanics theory, resulting in high cement volume in the mixture, which impairs the material greenness. High volume of supplementary cementitious materials (SCMs) has been used to mitigate the high carbon footprint of ECC. The SCMs used include fly ash, slags, silica fume, iron ore tailings, limestone, calcined clay, rice husk ash, and recycled fine powder [3, 11–17].

Among the SCMs used, fly ash (FA) has been demonstrated as the most appropriate one in ECC due to its good mechanical performance and wide availability. However, FA is expected to face a declining supply in the future due to the potential reduction of coal-fired power production [18]. Moreover, ECC performance is considerably influenced by the quality of FA, including compositions, particle size, and water requirement [15]. Sometimes high-quality FA that can be used for ECC is unavailable in some regions, such as Saudi Arabia. Therefore, an alternative green material to FA, which has abundant reserves and maintains the high performance of ECC is urgently needed.

Volcanic ash (VA) is a natural pozzolan, with ample availability in

* Corresponding author.
E-mail addresses: zhuhe@umich.edu (H. Zhu), hwhsiu@umich.edu (W.-H. Hu), mohammed.mehthel@aramco.com (M. Mehthel), thibault.villette@aramcouk.com (T. Villette), oscardaniel.salazarvidal@aramco.com (O.S. Vidal), waleed.nasser@aramco.com (W.N. Nasser), vcli@umich.edu (V.C. Li).

https://doi.org/10.1016/j.cemconcomp.2023.105051
Received 5 November 2022; Received in revised form 20 March 2023; Accepted 24 March 2023
Available online 29 March 2023

volcanic areas [19], as well as low-cost characteristics, which qualifies VA as a potentially attractive SCM for concrete. VA is the product of volcanic eruptions, which impose impacts on electricity networks, water systems, aviation, etc [20,21]. If not utilized effectively, VA may raise economic and environmental concerns.

VA has been explored in developing low-cost and durable concrete [19]. Different conclusions have been reached on the influences of VA on concrete performance. Most studies found a reduction in compressive strength when cement is partially replaced by VA [21–25]. The compressive strength decreases with the increased replacement ratio of VA to cement. Approximately 40% of strength reduction is observed when 40% of cement is replaced by VA [23]. A 10–30% replacement ratio has been suggested to minimize significant strength loss for concrete [26–28]. In contrast, a strength enhancement was reported for a concrete containing 30% cement substitution with fine VA (6 μm of average diameter) [22], attributed to the filling effect and increased pozzolanic activity of fine particles. Other researchers have reported improved durability for a concrete that substitutes 20% of cement substitution with VA, where about 6% of shrinkage and 20% of water sorptivity reduction were observed [21,24]. Meanwhile, both better and poorer performances of VA-concrete have been observed in sulfate environments [29,30]. In general, a low substitution range (10–30%) of cement by VA appears to attain acceptable strength and durability performance, while utilizing a higher volume of VA in concrete compositions remains a challenge.

To the best knowledge of the authors, no investigation on incorporating VA in ECC has been conducted. Specifically, the total replacement of fly ash (FA) with volcanic ash (VA) involves a large volume of VA in ECC composition, which brings about unknown challenges for the successful utilization of VA in ECC. VA has negative impacts on the fresh properties of concrete. When the VA replacement level is 20%, the slump diameter increases by 10–20%, and V-funnel flow time decreases by more than 50%, indicating decreased viscosity [25,31]. Also, an increased bleed tendency has been observed [32]. For VA incorporation in ECC, the control of rheology is even more vital since suitable viscosity is required for uniform dispersion of fibers [33–35]. Although up to 0.5% volume of polypropylene fiber has been successfully processed in a concrete incorporating 20% VA [24], the high volume of VA (up to 70%, as replacement of FA) and fiber (2% volume) exert extraordinary challenges in the processing of VA ECC.

Beyond the rheological properties, the composition requires deliberate composition tuning to maintain the superior mechanical performance of ECC, especially high tensile ductility, tight crack width, and self-healing capacity. To realize the potentially innovative low-cost and durable construction material, investigations on the composition and fresh and long-term properties of VA ECC are much needed.

The objective of this study is to develop a durable ECC by completely replacing fly ash with volcanic ash, providing a solution to the decreasing availability of high-quality FA. A comprehensive experimental research program including the characterization of rheological properties, compressive strength, uniaxial tensile performance, crack patterns, and self-healing capacity was initiated. This paper reports on the research findings, including the strategies of rheology and strength loss control. Specifically, a VA ECC with high ductility (>5%) and tight crack width (<100 μm) was developed. The mechanisms underlying the macroscopic properties of this new composite were investigated via mercury intrusion porosimetry (MIP), X-ray diffraction (XRD), and thermogravimetric analyses (TGA) methods.

2. Experimental program

2.1. Material and mix proportions

Twelve mixtures were designed to demonstrate the feasibility of volcanic ash ECC (VA ECC). The binder system includes ordinary Portland cement (OPC), fly ash (FA) or volcanic ash (VA), and silica fume (SF). The VA was obtained from the Jedda site in the western region of Saudi Arabia. Desert sand obtained from Saudi Arabia (Al-Hassa) was utilized with a 0.3 mass ratio of the binder. Table 1 lists the chemical compositions of binder constituents and Fig. 1 shows their particle size distribution.

The morphology of VA and FA can be found in Fig. 2. It is shown that VA particles are much more angular when compared to the spherical shape of FA. The VA particles also contain cracks and channels as well as pores. The particle size of VA is about an order of magnitude larger than the reference FA. The size and morphological differences between VA and FA are expected to lead to differences in paste rheology in the fresh state and mechanical properties in the hardened state.

The mix designs of ECCs for this study is shown in Table 2. Conventional FA-based ECCs were adopted as referenced mixtures, where three common ratios of the FA/OPC (0.6, 1.2, and 2.2) were used for different strength grade purposes, denoted as FA06, FA12, and FA22. Correspondingly, FA was completely replaced by VA to develop the FA-free ECC, denoting VA06, VA12, and VA22, respectively. To enhance the compressive strength, 120 kg/m^3 of silica fume (SF) [36] were incorporated in moderate strength VA ECCs, named MVA06, MVA12, and MVA22 in Table 2. For high-strength VA ECC (HVA06, 12, 22), the water to binder ratio was fixed at 0.2, while all other compositions adopted a 0.25 water/binder ratio.

For all ECC mixtures, 20 kg/m^3 of polyethylene (PE) fibers with 20 μm diameter, 12 mm length, 100 GPa Young's modulus, and 3 GPa tensile strength were employed as fiber reinforcement. Water reducer (WR, MasterGlenium 7920 from BASF) associated with hydroxypropyl methylcellulose (HPMC) was utilized for tailoring the fresh properties suitable for fiber dispersion. The dosages of WR and HPMC will be discussed in detail in Section 3.1, so they are not included in Table 2.

2.2. Sample preparations and test methods

The dry constituents (OPC, FA or VA, SF, sand, and HPMC if used) were pre-mixed for 5 min using a Hobart Planetary Mixer (Model: HL300, 28.4-L of volume). Then water associated with the water reducer (WR) was added and further mixed for 10 min at 100 rpm. Thereafter, a mini-slump cone (diameter $d_0 = 10$ cm) per ASTM C1437 [37] was used for the flow table test. After lifting the mini-cone, the paste spread on the flow table, and the spread diameter was measured once the paste came to a rest. In addition, the rheological properties of fresh pastes were measured using an ICAR Plus Rheometer (Fig. 3). The measured torque (T) and rotational speed (N) can be fitted on a regressed curve [38] as

$$T = G + HN + CN^2 \tag{2}$$

where G, H, C are the fitting parameters of the T-N relation. According to the Modified-Bingham model (M − B), the yield stress (τ) and viscosity (μ) can be derived by the Reiner–Riwlin equation [38]:

$$\tau = \frac{\left(\frac{1}{R_i^2} - \frac{1}{R_o^2}\right)}{4\pi h \ln\left(\frac{R_o}{R_i}\right)} G \tag{3}$$

$$\mu = \frac{\left(\frac{1}{R_i^2} - \frac{1}{R_o^2}\right)}{8\pi^2 h} H \tag{4}$$

Table 1
Chemical compositions of binder constituents measured by the X-ray fluorescence method (%).

Constituents	CaO	Al_2O_3	SiO_2	Fe_2O_3	MgO	SO_3	K_2O
OPC	63.5	4.8	19.6	2.9	2.2	2.6	0.6
SF	0.4	0.7	96.5	0.3	0.5	0.5	0.85
FA	10.8	16.2	51.6	5.0	3.7	1.4	2.5
VA	9.7	15.2	43.8	13.9	7.9	0	1.13

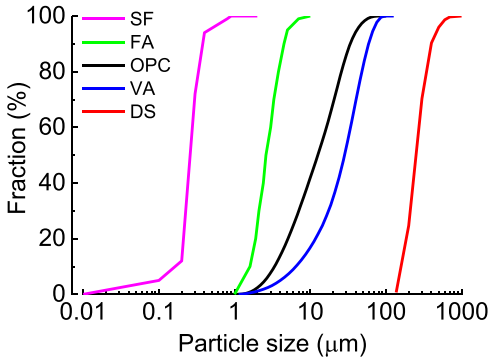

Fig. 1. Particle size distributions of dry constituents.

where R_i, R_o, and h are the vane radius, container radius, and vane height, corresponding to 63.5 mm, 75 mm, and 127 mm, respectively (Fig. 3).

Once the rheological test was completed, the paste was further mixed for 1 min. Then fibers were added to the fresh materials and mixed at 200 rpm for an additional 5 min. After obtaining a homogeneous fiber dispersion, the fresh ECC was cast into 50 mm-cube and dogbone-shaped molds (Fig. 4). Also, the spread diameter of ECC was measured by the flow table. Different from the paste's test (without vibrations), the flow table was dropped 25 times in 15 s per ASTM C1437 [37]. The spread diameter of paste and ECC was marked as D_{paste} and D_{ECC}, respectively.

After curing in air (20 ± 3 °C, 40 ± 5% RH) for 28d, the cube and dogbone-shaped specimens were used for compressive strength and uniaxial tension tests, where each test included 3 specimens per batch. Two linear variable displacement transducers (LVDT) were used to measure the tensile deformation of tensioned specimens (Fig. 4). The gauge length was approximately 80 mm (green part in Fig. 4(a)). Tensile ductility was calculated by dividing the deformation at peak load with the gauge length. Crack width was measured by a portable microscope during loading when the specimens were tensioned to 1%, 2%, 4%, and failure strain level.

2.3. Self-healing test

After tensile performance investigations in *Section 3.2*, −06 series ECC have marginally higher tensile strength, while −22 series ECC has much lower tensile strength than −12 series ECC. Hence, mixtures of FA12, VA12, MVA12, and HVA 12 were selected for self-healing tests. Following 28 days of curing in air (20 ± 3 °C, 40 ± 5% RH), 3 dogbone samples of each mix were tensioned to failure, denoted as 28d-Ref. Three series of samples were pre-tensioned to 0% (without loading), 1%, and 2% strain levels, which were then cured in 7 cycles of 24 h of water and 24 h of dry curing (20 ± 3 °C, 40 ± 5% RH). Unlike the bacteria healing [39] or crystalline admixtures [40] method may have long-term healing, the autogenous healing mechanism of ECC is primarily caused by the $CaCO_3$ precipitation and the continuous hydration, which has been demonstrated to be completed in the first 7–14 days [7,13,36].

Self-healing samples were named 0%-heal, 1%-heal, and 2%-heal, respectively, and each series included 3 samples. As this study focuses on comparing the healing ability of VA ECC to FA ECC, only the healing degree of crack closure after healing was investigated instead of the whole healing process. The unloaded crack width of pre-tensioned specimens was measured by a microscope at the beginning and by the end of wet-dry curing. The recovery ratio crack surface is employed to quantify the healing degree of crack width, which can be calculated by equation (5) [3]. Besides the surface crack closure rate, the healed tensile performance was also investigated. After 7 wet-dry curing cycles, the healed specimens were tensioned to failure following the same procedure in *Section 2.2*.

$$\text{Recovery ratio} = \left(1 - \frac{\textit{crack width after healing}}{\textit{crack width before healing}}\right) \times 100\% \quad (5)$$

2.4. Micro/mechanism investigation

Fibers influence the pore structures of ECC significantly, which may conceal the effect of ECC constituents, such as VA [41]. Therefore, ECC pastes without fibers were cast into 50-mm cube molds to interpret the

Table 2
Mixture design of ECC (kg/m^3).

Mixture	OPC	FA	VA	SF	Sand	Water
FA06	800	480	0	0	384	320
FA12	600	720	0	0	396	330
FA22	400	880	0	0	384	320
VA06	800	0	480	0	384	320
VA12	600	0	720	0	396	330
VA22	400	0	880	0	384	320
MVA06	800	0	480	120	420	350
MVA12	600	0	720	120	432	360
MVA22	400	0	880	120	420	350
HVA06	800	0	480	120	420	280
HVA12	600	0	720	120	432	288
HVA22	400	0	880	120	420	280

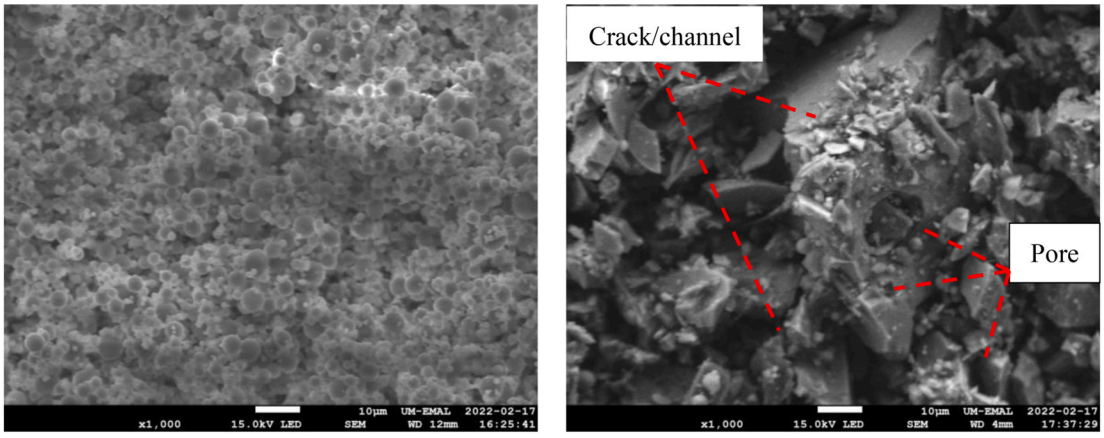

Fig. 2. SEM of (a) FA and (b) VA, showing crack/channel and pores.

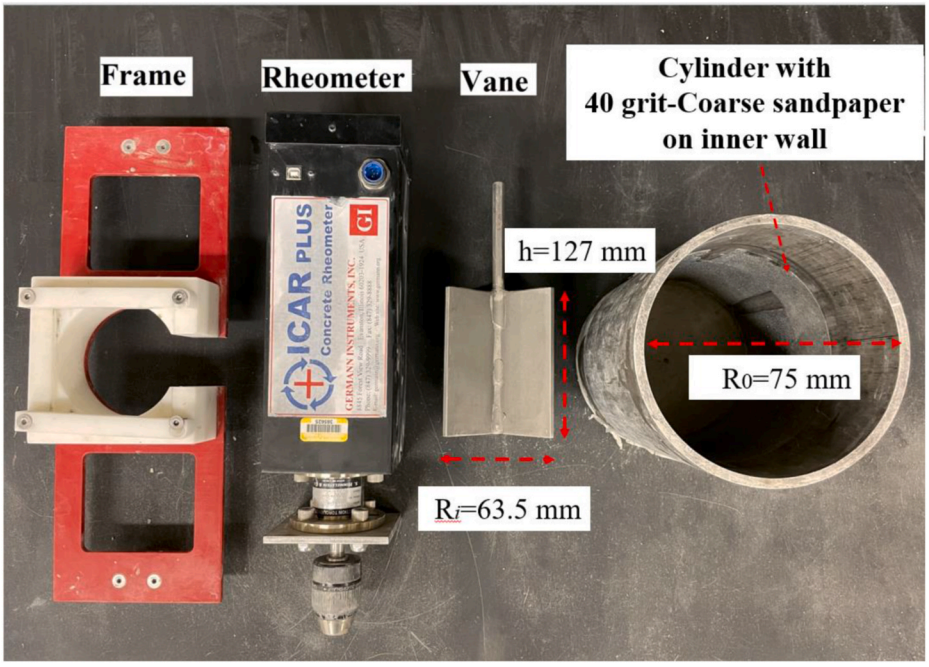

Fig. 3. Icar plus rheometer [9].

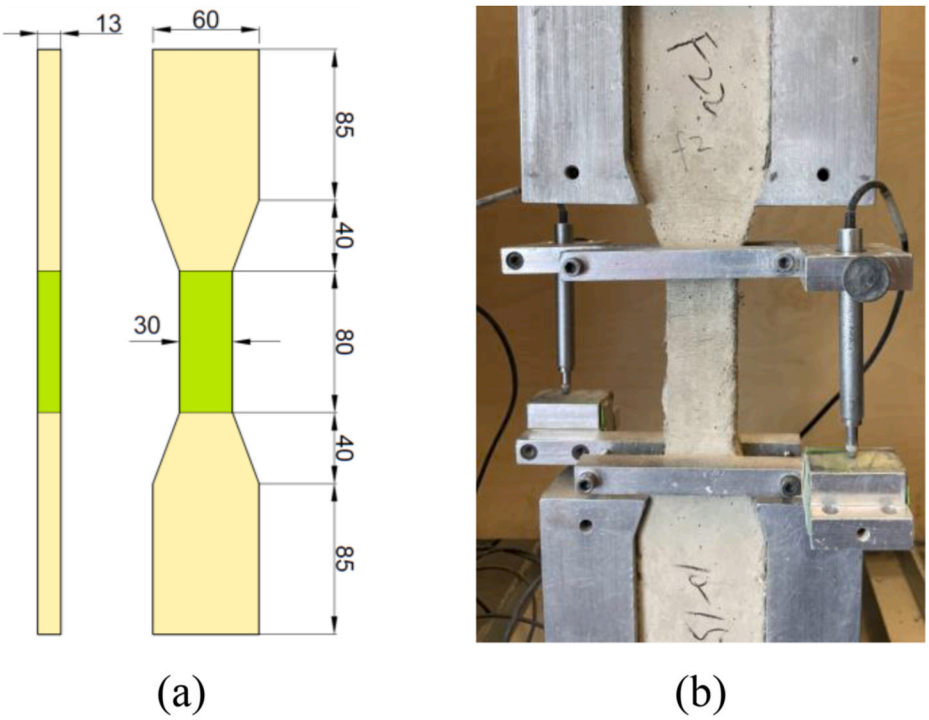

Fig. 4. Dogbone-shaped specimen for uniaxial tension (a) showing dimensions (Unit: mm) and (b) the grip and LVDT set up during loading.

underlying mechanism of macro-mechanical behaviors. After 28 days of air curing, the cube samples were crushed into small pieces (about 5 mm chunks). For the pore structures test, the chunk samples were fully immersed in isopropanol for 7 d as suggested by solvent exchange method, and then dried in a vacuum desiccator [42,43]. Then Micromeritics AutoPore V Mercury Porosimeter was used to perform the pore structure analysis up to 420 MPa pressure, where the mercury-cement contact angle is 130°.

While the solvent exchange method may influence the calcium hydroxide (CH) amount tested by thermogravimetric analysis (TGA) [42], 5-mm chunks, already air-cured for 28 d, were dried in a 60 °C oven for 7 d as used in the literature [44]. Although oven drying may accelerate the carbonation of samples [42,44], the objective of comparing the CH difference among different mixtures in this study can be met. More details will be discussed in *Section 3.4.3*. After 7 d of oven drying, the samples were pulverized and passed a 75-μm sieve to obtain powder samples for TGA and X-ray diffraction (XRD) tests. 10 mg of each powder sample was performed TGA tests, heated from 20 °C to 950 °C at a rate of 10 °C/min under the N_2 gas atmosphere. For XRD analysis, the powder sample was front-loaded and scanned between 10° and 40° 2θ at

a rate of 2°/min using a Rigaku Ultima IV instrument by CuKα radiation.

3. Results and discussions

3.1. Rheological engineering

In light of the significant difference in morphology and particle size of VA in comparison to that of FA (Fig. 2), the uncertainty of the VA effect on paste rheology and impact on fiber dispersion has been increased. Since VA06 tends to affect the rheology less, moderate VA content (VA12) and high VA content (VA22) were examined with trial amounts of WR and HPMC. Meanwhile, the effect of silica fume was also investigated by MVA 12. These trial compositions will guide the formal mixing of VA ECC influenced by VA and SF volume. After obtaining the suitable rheology range for ECC (*Section 3.1.1*), the fresh properties including spread diameter and rheology parameters for all compositions were analyzed (*Section 3.1.2*).

3.1.1. Results of trial compositions

Table 3 lists the results of trial tests on viscosity control and its effect on fiber dispersion. It is difficult to quantify ECC's fiber dispersion uniformity during the mixing process. The mixing quality (Table 3) was first evaluated by eyes empirically. Since fiber clumps are known to impair the tensile performance of ECC [33,45], eye examination screened out the unqualified mixtures as a first step. Then the mixtures without fiber clumps were further examined by uniaxial tensile performance (values and variability of strength and ductility) to narrow down the appropriate viscosity range. This is the strategy and significance of conducting trial rheology tests.

It should be noted that the negative value has no physical meaning, which is a measurement error caused by segregated paste. Regarding VA12_T1, 8 kg/m^3 of WR was found to be the lowest dosage for material liquefaction. However, the liquefied paste exhibited severe segregation, with some heavier constituents deposited on the bottom with light materials floating on the top (Fig. 5 (a)). To overcome the segregation problem, 0.05% binder weight (0.7 kg/m^3) of HPMC [9] was employed in VA12_T2 to increase the paste viscosity to 21.5 Pa s. Consequently, a homogeneous and cohesive paste was obtained (Fig. 5 (b)).

With the increase of WR from 9 kg/m^3 to 12 kg/m^3 in VA12_T3, the paste viscosity decreased to 6.0 Pa s. Both VA12_T2 and VA12_T3 demonstrated good fiber dispersions, as well as a superior tensile performance (Fig. 6 (a)). Hence, HPMC successfully modified the segregated paste to a homogeneous paste. A paste viscosity of 6.0–21.5 Pa s is suggested as suitable for PE fiber dispersion.

Increased VA volume magnifies the challenge of material mixing. At least 16 kg/m^3 of WR is needed to liquefy the VA22_T1 paste. Similar to VA12_T1, segregation and sedimentation were observed in the resulting paste. The viscosity was increased to 9.1 Pa s by including 0.05% binder weight of HPMC (0.7 kg/m^3) in VA22_T2, leading to good fiber dispersion during mixing. With the WR dosage further increased to 21 kg/m^3 in VA22_T3, the viscosity diminished to 0.7 Pa s, resulting in insufficient viscosity and the appearance of minor paste segregation and fiber balling during mixing. However, the reduced viscosity could be restored by increasing the HPMC content. 0.1% binder weight of HPMC (1.3 kg/m^3 in VA22_T4) increased the viscosity to 8.6 Pa s, enabling good fiber dispersion during mixing. VA22_T2 and VA22_T4 exhibited comparable tensile results (Fig. 6 (b)).

Increased fluidity due to large WR dosage reduced the stability or viscosity of the paste, resulting in the tendency of segregation and sediment, while HPMC's long chain polymer augmented the viscosity of the paste [46]. Although pastes with different ratios of WR and HPMC were designed for different VA contents, comparable viscosity was obtained, ensuring good fiber dispersion and robust strain hardening effect (Fig. 6).

Silica fume improves the fresh property of VA-based ECC considerably. Although no HMPC was used in MVA_T1, a homogeneous and cohesive paste was obtained without segregation or sediment, as observed in VA12_T1 and VA22_T1. However, the viscosity (2.2 Pa s) of MVA_T1 was found inadequate for polyethylene fiber mixing, where minor fiber clumps were observed. Viscosity was enhanced to 8.9 Pa s with the inclusion of 0.7 kg/m^3 of HPMC, resulting in the higher tensile ductility of MVA_T2 compared to MVA_T1 (Fig. 6 (c)).

In general, 0.05% binder weight of HPMC (0.7 kg/m^3) combined with a suitable amount of WR tuned to VA content was found suitable for overcoming the segregation of VA-based ECC while maintaining its viscosity with at least 6 Pa s for PE fiber dispersion. The details of the formal mixtures can be found in the following section.

Table 3
Trial tests of rheology control by different amounts of HPMC and WR.

Mix ID	HPMC (kg/m^3)	WR (kg/m^3)	Viscosity (Pa•s)	Mixing quality
VA12_T1	0	8	−6.0*	Paste segregation, bottom sediment as shown in Fig. 5 (a)
VA12_T2	**0.7**	**9**	**21.5**	**No fiber clumps were found by hand examination**
VA12_T3	**0.7**	**12**	**6.0**	**No fiber clumps were found by hand examination**
VA22_T1	0	16	−0.7	Paste segregation, bottom sediment. Similar status is shown in Fig. 5 (a)
VA22_T2	**0.7**	**18**	**9.1**	**No fiber clumps were found by hand examination**
VA22_T3	0.7	21	0.7	Minor paste segregation by visual examination
VA22_T4	**1.3**	**21**	**8.6**	**No fiber clumps were found by hand examination**
MVA12_T1	0	8	2.2	Minor fiber clumps **by hand examination**
MVA12_T2	**0.7**	**12**	**8.9**	**No fiber clumps were found by hand examination**

3.1.2. Fresh properties of formal compositions

Table 4 lists the fresh properties of the formal mixtures, including FA ECC, VA ECC, MVA ECC, and HVA ECC. By controlling the viscosity beyond 6 Pa s, all mixtures are successfully prepared with cohesive paste and good dispersion of PE fibers during mixing. Li et al. [33] suggest that a viscosity larger than 6.5 Pa s is suitable for PVA fibers. Meanwhile, Yang et al. [47] find that controlling the viscosity above 3 Pa s can obtain robust strain-hardening ECC with PVA fibers, and tensile performance increases with the viscosity increase. Similarly, 4–8 Pa s of viscosity have been demonstrated suitable for mixing PE/PVA hybrid fibers [9]. Therefore, 6 Pa s is suggested and established a minimum viscosity for mixing PE ECC.

HVA ECC possesses much higher viscosity (25.2–29.9 Pa s) than other mixes in Table 4 (6.0–11.0 Pa s). The increased viscosity was caused by the low water/binder ratio of HVA (0.2), and water bleeding was observed when more WR was used. Also, the static yield stress of HVA ECC was higher than VA ECC and MVA ECC. As a result, the spread diameter of HVA ECC was lower than VA ECC and MVA ECC.

The inclusion of a large volume of VA undermined the fresh properties of ECC paste. Distinct from ECC with VA, FA-ECC attained a viscosity of 6.5–8.0 Pa s with no HPMC and only a very small amount of WR (approximately 2 kg/m^3). Some contradictory findings were reported in the literature regarding the effect of VA on workability. Increased flowability was found for up to 30% cement replacement by VA [25,31]. In contrast, increased WR demand and low workability retention were

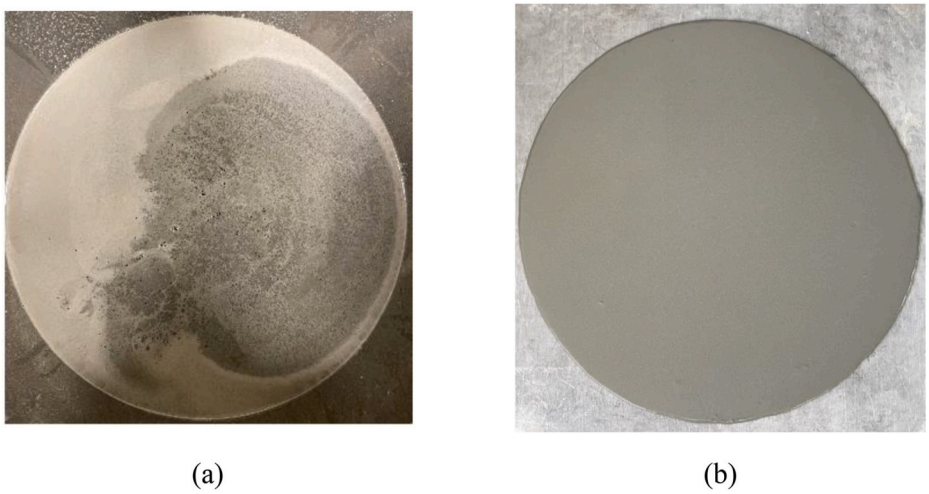

Fig. 5. Paste status after mixing with different combinations of HPMC and WR. (a) V12_T1 paste shows segregation, with darker color VA and lighter color cement, and (b) V12_T2 paste shows homogeneity and cohesiveness.

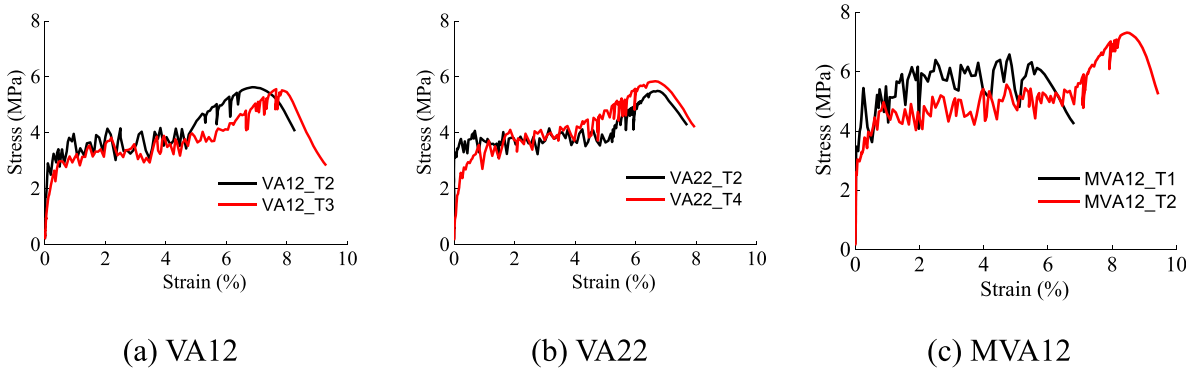

Fig. 6. Representative tensile stress-strain curve of trial mixes.

Table 4
The fresh properties of formal mixtures.

	WR (kg/m^3)	HPMC (kg/m^3)	Viscosity (Pa•s)	Static yield stress (Pa)	D_{paste} (mm)	D_{ECC} (mm)
FA06	2.0	0	6.5	125.7	170	175
FA12	1.8	0	7.5	137.4	174	178
FA22	1.8	0	8.0	131.7	170	176
VA06	8	0.7	6.5	17.0	270	165
VA12	12	0.7	6.0	18.4	266	165
VA22	18	0.7	8.6	19.4	267	170
MVA06	12	0.7	10.5	34.0	245	160
MVA12	12	0.7	8.9	32.9	250	155
MVA22	15	0.7	11.0	37.1	245	155
HVA06	21	0.7	29.9	69.4	220	155
HVA12	22	0.7	25.2	50.2	220	155
HVA22	21	0.7	26.9	46.2	235	150

observed for concrete with 15% weight of VA [18]. Moreover, decreased viscosity [48] and aggravated bleeding [32] were reported for VA-incorporated concrete. In this study, a large volume of VA was utilized for completely replacing FA, rather than substituting for cement, which may lead to different phenomena compared to those observed in previous studies.

The angular particle morphology of VA (Fig. 2) increased the friction between particles during mixing. In addition, pores and cracks in VA particles increased the demand for water/WR during mixing. The porous VA particles were consistent with the observation from a previous study [49]. In contrast, the solid spherical shape of FA particles (Fig. 2) revealed a lubricating effect that reduced the water demand for liquefaction. The angular and porous morphology were responsible for the impaired fresh properties of VA ECC compared to FA ECC.

FA ECC has significantly higher static yield stress (125.7–137.4 Pa). As a result, the spread diameter of FA paste without fibers (around 170 mm) was found considerably lower than that of VA paste (260–270 mm). The low workability of concrete incorporating VA was also reported in a previous study [18]. While the viscosity affects the quality of fiber dispersion, the yield stress dominates the shape retention ability, such as the build-up thickness in sprayed concrete/ECC and the layer build-up speed of 3D printed concrete/ECC [35,50]. Relative low static yield stress of VA paste indicates potential limitations of VA-ECC in shotcrete and 3D printing applications compared to FA-ECC, which requires further investigations in future studies.

3.2. Mechanical performance

3.2.1. Compressive strength

With FA completely replaced by VA, VA ECC showed a considerable reduction of compressive strength compared to FA ECC (Fig. 7). FA06 and FA12 had comparable compressive strengths of 54.1 MPa and 53.9 MPa. However, the compressive strength of FA22 dropped to 39.2 MPa. Similarly, the compressive strength of VA 06 (37.9 MPa) was slightly higher than VA12 (33.9 MPa), while VA22 experienced a significant reduction of strength to 24 MPa. This phenomenon was also observed in

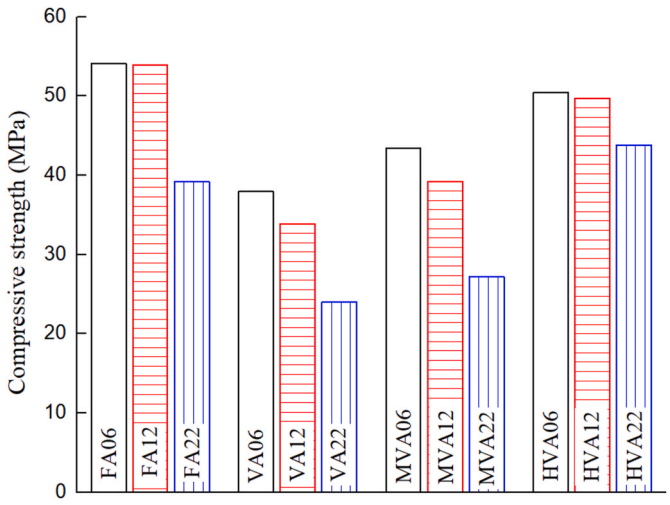

Fig. 7. Compressive strength of VA ECC at 28 d. FA ECC served as a reference mix.

MVA and HVA. Increasing the VA/OPC or FA/OPC ratio from 0.6 to 1.2 had little impact on the compressive strength while improving the material's greenness. Although the ECC could be greener by increasing the VA/OPC or FA/OPC ratio from 1.2 to 2.2, the compressive strength was significantly impaired.

Adding SF in compositions restored part of the strength loss, MVA ECCs attained 43.4, 39.2, and 27.2 MPa in MVA06, MVA12, and MVA22. MVA ECCs gained approximately 15% of compressive strength compared to that of VA ECCs. The compressive strength was further enhanced by reducing the water/binder ratio from 0.25 to 0.2 in HVA. The compressive strength of HVA06, HVA12, and HVA 22 was 50.4, 49.7, and 43.8 MPa. HVA ECCs obtained a compressive strength comparable to those of FA ECCs.

3.2.2. Tensile results

Fig. 8 shows tensile stress-strain curves and Table 5 summarizes the characteristic tensile values of the developed ECCs at 28 d. Regardless of the mix compositions, comparable tensile strength and tensile strain capacity were observed between the −06 and −12 series, where −06 and −12 represent the VA or FA to OPC ratio are 0.6 and 1.2. This finding is consistent with that of their compressive strengths.

FA22 showed a reduction of the ultimate tensile strength (5.3 MPa) and ductility (5.4%) compared to FA 12 (7.7 MPa and 6.6%). Different from the compressive strength, VA22 had higher tensile strength (5.6 MPa) and tensile strain capacity (6.7%) than those of FA22. Moreover, the tensile strength increased to 5.7 MPa (MVA22) and 7.5 MPa (HVA22) with denser matrices. Meanwhile, the tensile strain capacity augments to 7.6% and 8.7% for MVA22 and HVA22, respectively. The addition of SF and reducing the water/binder ratio improved both tensile strength and ductility.

3.2.3. Crack patterns

Fig. 9 shows representative crack patterns of the developed ECC at failure. All developed ECCs showed multiple tiny cracks regardless of the use of FA or VA. Crack number, average crack width, and maximum crack width are summarized in Table 5. When the FA to OPC ratio increased from 0.6 to 2.2, the crack number at failure also increased from 89 to 97. FA series ECCs exhibited the smallest crack width among all mix series. FA06 and FA22 had average crack widths of 51 μm and 40 μm, respectively.

Fig. 10 (a) illustrates the crack width distribution of ECCs with different VA replacement ratios. There is a clear trend that higher VA volume resulted in smaller cracks. For example, the cracks of VA 22 were mainly distributed between 0 and 40 μm together with 11 cracks at 40–60 μm. In contrast, most of the cracks of VA06 were in the range of 40–80 μm.

Different SCMs affect ECC's crack width. VA ECCs had a slightly lower crack number compared to FA ECC, and a marginally larger average crack width (59 μm, 50 μm, 46 μm for VA06, VA12, and VA22, respectively). Fig. 10 (b) shows the crack distribution of ECCs with different SCMs. FA12 had smaller cracks than other compositions, mainly distributed in the range of 0–60 μm. Adding silica fume in MVA contributed to more cracks (90–98) at failure with a comparable average crack width to VA ECC (Table 5). Fig. 10 (b) also shows that VA12 and MVA12 had similar crack width distributions in the range of 20–60 μm. This indicates the advantages of silica fume in MVA that enhance both strength and ductility while maintaining a similar crack pattern. However, reducing the water to binder ratio significantly increased the crack width of HVA ECC. Specifically, HVA06 and HVA22 had average crack width of 91 μm and 82 μm, almost twice that of FA ECCs. The crack distribution results (Fig. 10(b)) demonstrate that HVA12 had 10 cracks in 20–40 μm range, and most of the cracks were larger than 60 μm for HVA12.

The crack numbers distribution versus crack width data of FA ECC, VA ECC, MVA ECC, and HVA ECC (Fig. 10) can be fitted with a lognormal distribution probability density function, as proposed in previous studies [51–53]. Moreover, the lognormal distribution fits the crack distribution at different strain levels (Fig. 11). The lognormal distribution probability density function ($P(\delta,\varepsilon)$) at given crack width (δ) and strain level (ε) can be mathematically expressed by Eq. (6) [51–53].

$$P(\delta,\varepsilon)=\frac{1}{\delta\sigma\sqrt{2\pi}}e^{\frac{-(\ln\ \delta-\mu)^2}{2\sigma^2}} \tag{6}$$

where the parameters μ and σ can be calculated by the mean (m) and standard deviation value (s) of the crack widths following:

$$\mu=\ln\left(\frac{m^2}{m^2+s^2}\right),\sigma=\sqrt{\ln\left(\frac{s^2}{m^2}+1\right)} \tag{7}$$

with the increased ratio of VA replacement for OPC, more tiny cracks below 40 μm were observed. The crack numbers with a width larger than 100 μm increased slightly. While the crack numbers increased with the strain levels (from 1% to failure strain at 6–8%), most cracks retained widths between 0 and 80 μm (Fig. 11).

3.3. Self-healing results

The VA-based ECCs demonstrated self-healing capacity regarding crack recovery and mechanical enhancement. Fig. 12 presents the crack recovery ratio and crack width relationship of different ECCs after 7 wet-dry cycles. The self-healing capacity of ECC is influenced by the crack width, Ca^{2+} content, pre-damaged degree, and further hydration potential [7]. The crack recovery ratio in Fig. 12 mainly depends on the crack width and Ca^{2+} content since each composition utilizes identical OPC dosage and experiences the same preloading history. Crack recovery can be classified into 3 categories including full recovery, partial recovery, and negligible recovery. As shown in Fig. 12, cracks below 20 μm were almost fully healed (80–100%), and those cracks between 20 and 50 μm were partially healed (20–80%), while nearly no healing was observed for the cracks larger than 50 μm. The crack width and recovery ratio relationship is consistent with previous studies [7,13,36].

Although VA12 had a slightly higher average crack width than FA 12 (Table 5), VA12 proved a crack recovery capacity comparable to that of FA12. MVA12 exhibited a compromised healing capacity to VA12, where most cracks between 20 and 50 μm experienced below 50% of recovery ratio (Fig. 12 (C)). The details reasons related to the portlandite content in hydration products will be discussed by TGA results in Section 3.4. Moreover, limited healings were found in HVA12 due to its large

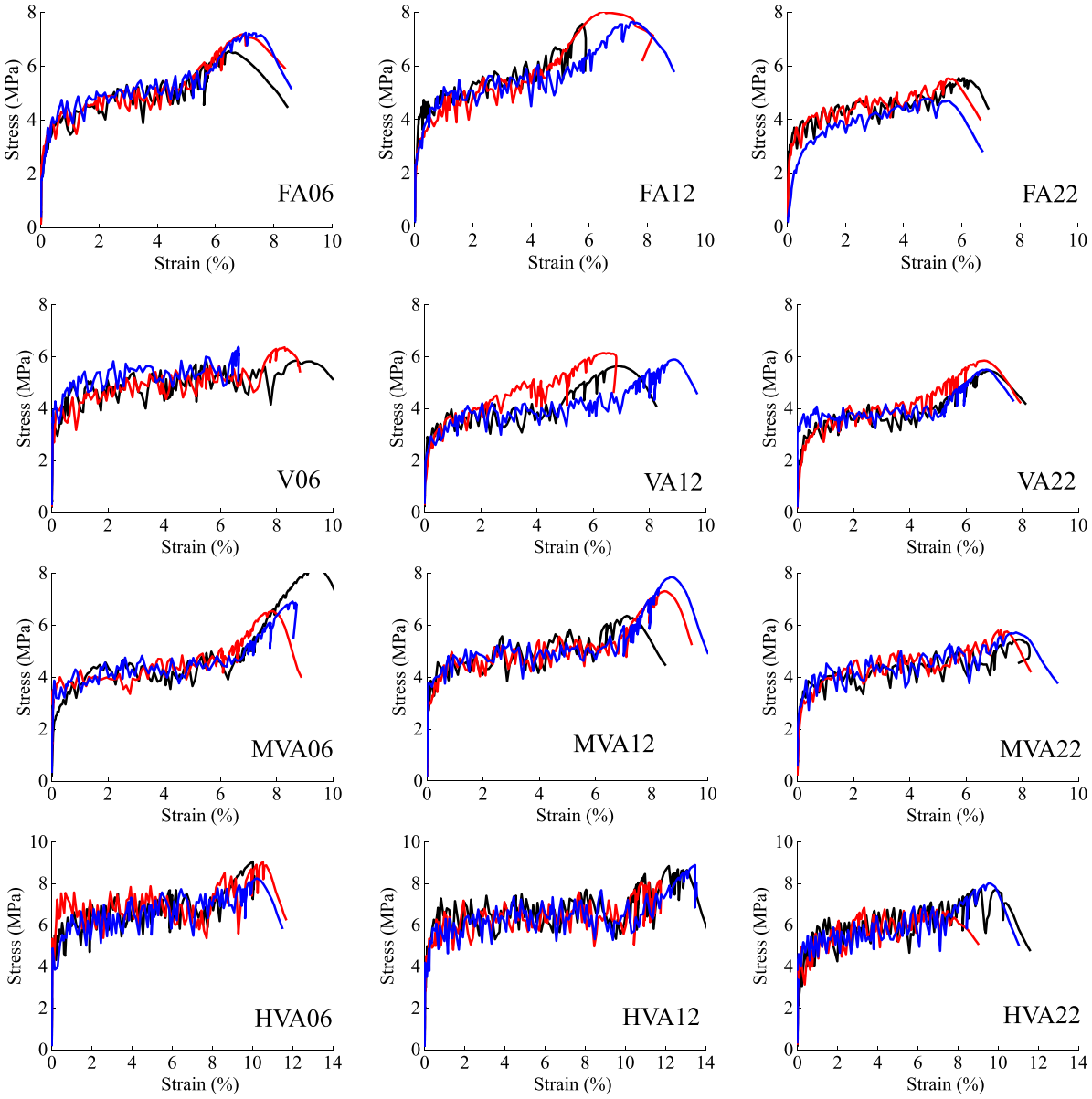

Fig. 8. Tensile stress-strain curves at 28 d.

Table 5
Summary of tensile results (strength, ductility, crack number, and width).

	Ultimate tensile strength (MPa)	Tensile strain capacity (%)	Crack No. at failue	Average crack width (μm)
FA06	7.0	6.8	89	51
FA12	7.7	6.6	92	43
FA22	5.3	5.4	97	40
VA06	6.2	7.9	85	59
VA12	5.9	7.4	89	50
VA22	5.6	6.7	84	46
MVA06	7.2	8.6	98	55
MVA12	7.2	8.1	91	51
MVA22	5.7	7.6	90	48
HVA06	8.8	10.3	78	91
HVA12	8.6	12.5	90	87
HVA22	7.5	8.7	64	82

crack width distribution (mostly larger than 40 μm).

There are some contradictory findings on the healed crack width of ECC. Yu [36] obtained a similar conclusion to this study, that cracks under 20 μm can be sealed well, and the cracks between 20–30 μm were 50–80% sealed. Moreover, the maximum healed crack width can be up to 30 μm [13] or 50 μm [54]. Curing environments, such as hot water, Ca$(OH)_2$, and Na_2SO_4 also promote the healing process [8,55]. However, Zhu et al. [13] observed that the crack exceeded 60 μm had a negligible healing effect, which is consistent with the findings in this study. It should be noted that some healing enhancement agents, such as bacteria, crystalline admixture, and encapsulated agents can improve the healable crack width even more than 100 μm [4,39,56,57]. Crack healing degree is crucial for water permeability, suggesting the need for crack control under 50 μm or even 20 μm when utilizing VA ECCs for water infrastructures.

Beyond crack healing reflected by the recovery ratio in Fig. 12, mechanical enhancement after wet-dry curing was examined for VA ECCs (Fig. 13). Due to the existence of unhydrated cement grains in the compositions, further hydration contributes to tensile strength development after curing in wet-dry cycles. The tensile strength of 0%-heal (no preloading but exposed to healing wet-dry environment) for VA12 increased to 8.2 MPa after wet-dry curing compared to 5.9 MPa at 28 d (without wet-dry curing). FA12, MVA12, and HVA12 showed a similar

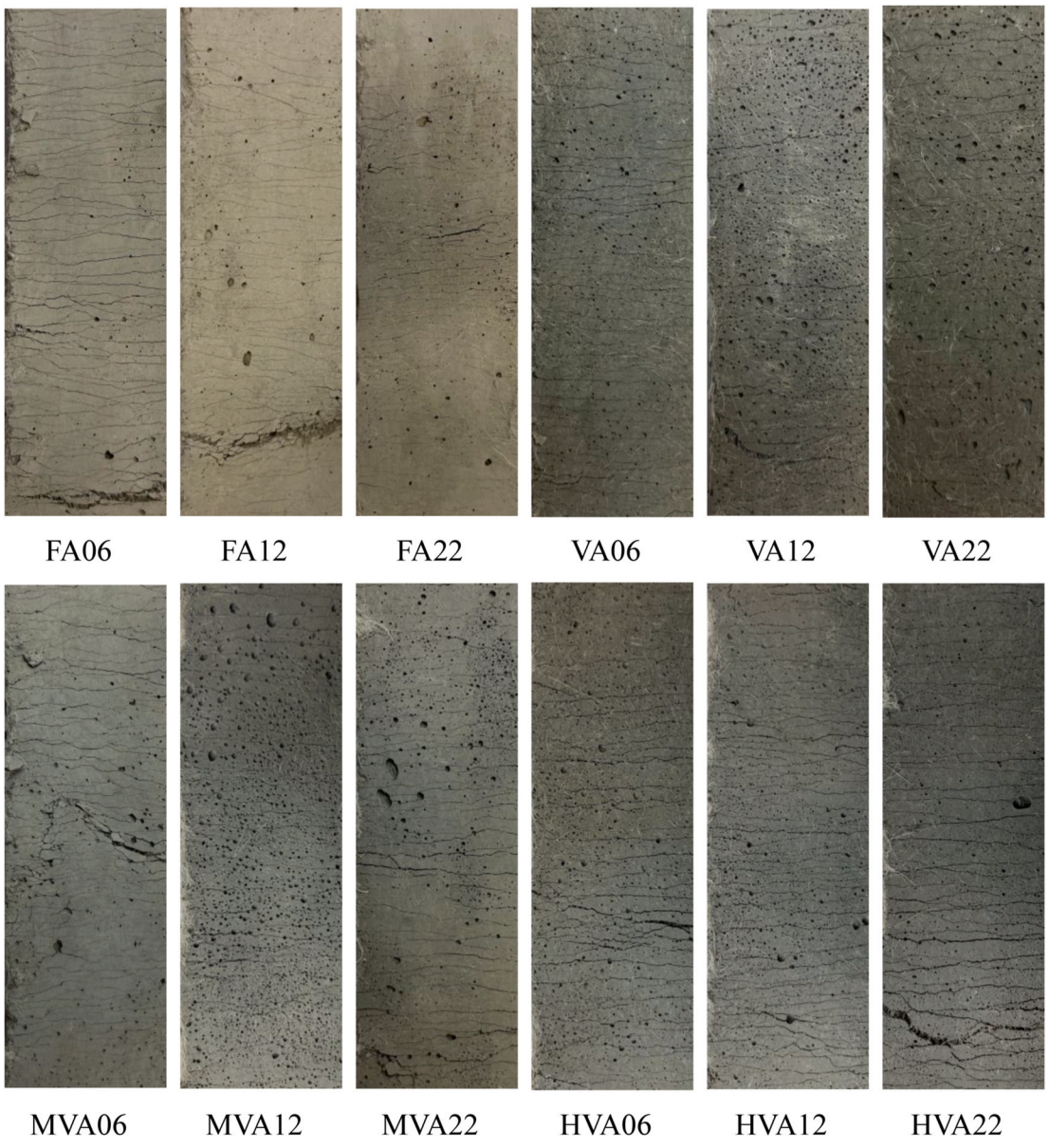

Fig. 9. Representative crack patterns of the developed ECC at failure corresponding to the 80-mm rectangle part of the dogbone specimen.

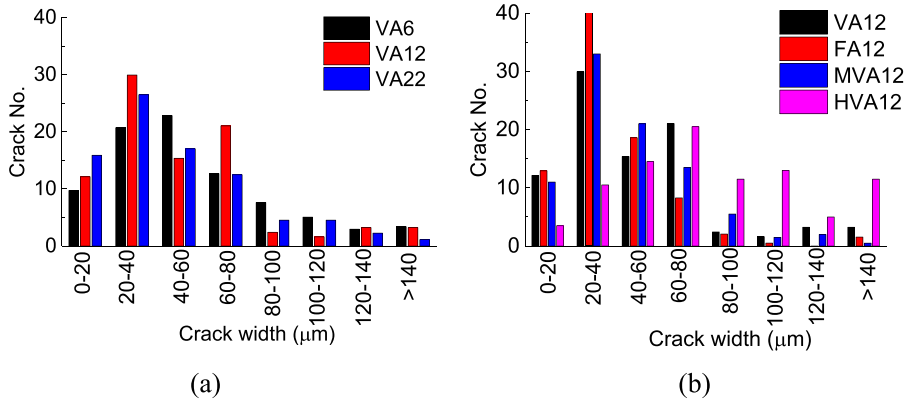

Fig. 10. The crack number distribution of different ECC at specimen failure, showing (a) the effect of VA content, and (b) the effects of FA, VA, SF, and W/B.

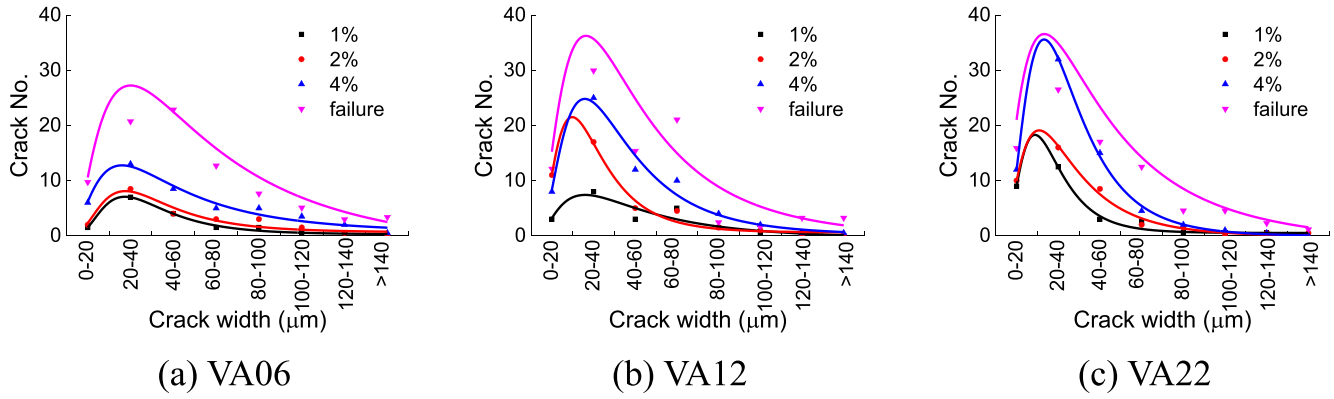

Fig. 11. Lognormal distribution of cracks for VA ECCs at different strain levels.

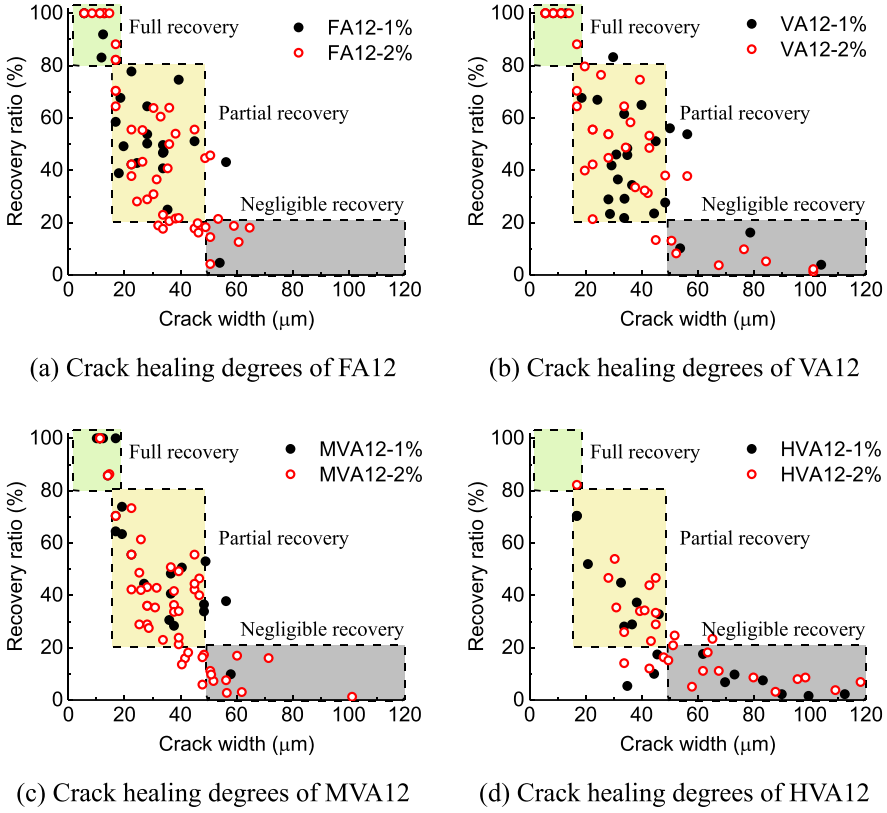

Fig. 12. Crack recovery ratio versus crack width for ECCs. (Note: The crack width of FA12, VA12, and MVA12 were all below 120 μm, while two cracks larger than 120 μm were observed in HVA12, which obtained negligible heals and were not shown to maintain the same X-axis range of figures.)

enhancement after wet-dry curing. The ultimate tensile strength of ECC is determined by the maximum fiber-bridging stress, which is further controlled by the fiber-matrix bonding. Since wet-dry cycles lead to further hydration, the densified matrix enhances the fiber-matrix bonding, explaining the increase of ultimate tensile strength after wet-dry curing.

The 1% or 2% pre-tensioned specimens show a comparable or marginally lower tensile strength compared to the virgin specimens (0%-heal) after wet-dry healing environment. Guided by the micromechanics design theory of ECC [3], cracks are initiated from smaller and smaller flaws at increasingly higher tensile stress. For the preloaded specimens, microcracks have already been initiated at sites of the large and moderate flaws, while smaller pre-existing flaws remain. The uncracked parts of the pre-tensioned specimens experienced identical further hydration to the virgin specimen after 7 wet-dry cycles. Therefore, the flaws distribution and fiber-matrix bonding experienced identical evolution between the virgin specimen and uncracked parts in the pre-tensioned specimen, resulting in comparable ultimate tensile strength between virgin and cracked specimens. This proves the advantage of ECC for maintaining the ultimate tensile strength with pre-damages.

Distinct from tensile strength, tensile ductility showed different degrees of reduction among the four mixes (Fig. 13). FA12 and VA12 had comparable ductility among 28d-Ref, 0%-heal, and 1% heal, and slight reduction for 2%-heal. MVA12 and HVA 12 showed obvious reduction among 28d-Ref, 0%-heal, 1% heal, and 2%-heal. Previous studies also found that the healed ECC obtained an increased tensile strength while a decreased tensile ductility [13,55,57]. There are two competitive

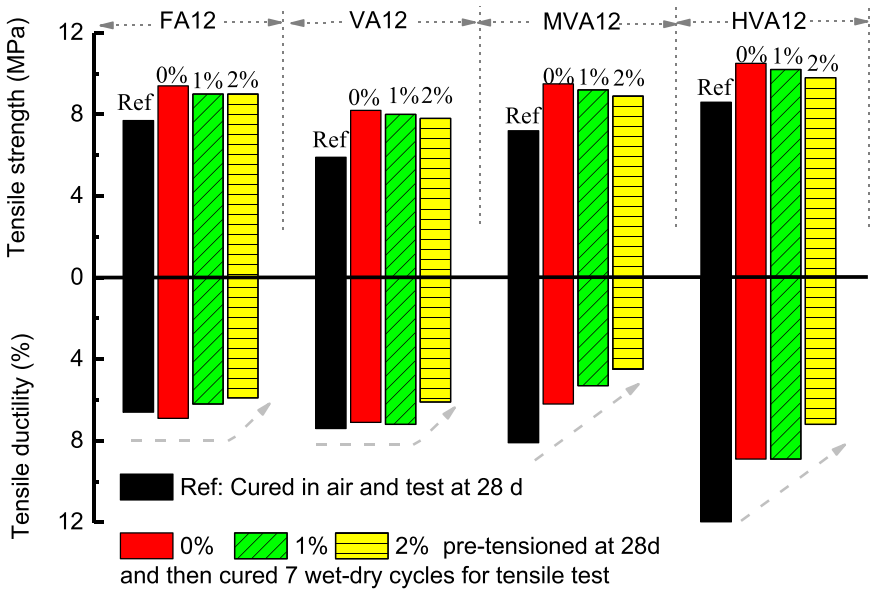

Fig. 13. Tensile strength and ductility of samples with and without wet-dry cycle healing.

mechanisms of wet-dry curing on tensile ductility performance. Further hydration increases the fiber-matrix bonding and fiber bridging stress, while refined pore structures diminish the flaw sizes, resulting in fewer cracks that can be activated under tension. Due to the nano-particles and high pozzolanic activity of silica fume, the refined pore structures play prevailing roles over the enhancement of fiber-matrix bonding, leading to the considerable ductility reduction in MVA12/HVA12 compared to FA12/VA12.

The reduced crack number at failure after wet-dry curing supports the hypothesis of diminished ductility due to refined flaws. Regarding the virgin specimen, 28d-Ref (before wet-dry curing) had more cracks than 0%-heal (after wet-dry curing). While the crack number of virgin specimens diminished from 92 to 72 for FA12, 40–60% reductions were found for VA-based ECCs (Table 6). Moreover, a marginal difference of the crack number at failure among 0%-heal, 1%-heal, and 2%-heal was observed. This further demonstrates that the pre-cracked specimens and virgin specimens possess similar flaw size distribution after wet-dry curing, resulting in the same crack initiations under tension, which is consistent with the results of the comparable ultimate tensile strength (Fig. 13).

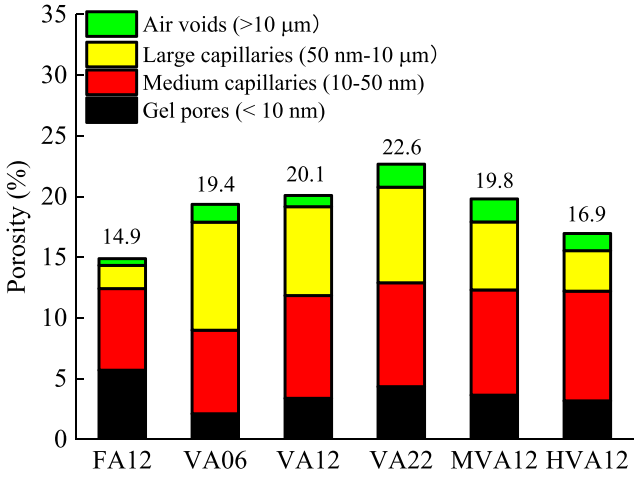

Fig. 14. The porosity distribution with different pore structures.

3.4. Micro/mechanism analysis

3.4.1. Micropore structures by MIP

The MIP-measured porosities (Fig. 14) of the different mixes are consistent with the compressive strength results presented in *Section 3.2.1* - larger porosity corresponds to lower compressive strength. For example, FA12 exhibited the lowest porosity (14.9%) while attaining the highest compressive strength 53.9 MPa compared to other mixtures.

Table 6
The healing effect on the crack number and average crack width of ECCs.

	Crack number				Average crack width (μm) (ductility*gauge length/crack number)			
	28d-Ref	0%-heal	1%-heal	2%-heal	28d-Ref	0%-heal	1%-heal	2%-heal
FA12	92	72	63	65	43	78	79	71
VA12	89	52	57	52	50	111	100	93
MVA12	91	51	45	46	51	98	95	83
HVA12	90	40	41	38	87	180	176	156

Increasing the VA to OPC ratio from 0.6 to 2.2 led to an increase in porosity from 19.4% to 22.6%. Although MVA12 had marginally lower porosity than VA12, a 15% improvement of compressive strength was obtained by MVA12 due to its reduced volume of large capillary pores and increased gel pores. Similarly, reduced large capillary pores were observed in FA12 and HVA12, contributing to the strength enhancement.

3.4.2. XRD results

XRD results (Fig. 15) reveal that VA (VA06, VA12, and VA22) based ECC and FA-based ECC possess similar mineral products, including portlandite ($Ca(OH)_2$ or CH), quartz (SiO_2), calcite ($CaCO_3$), as well as unhydrated CS (tri-calcium silicate and bi-calcium silicate). These minerals were commonly observed in OPC hydration products. The presence of dolomite ($CaMg(CO_3)_2$) peak was observed in VA-based ECC (VA06, VA12, and VA22), but was absent in FA12. VA contains a high amount of MgO in its composition (Table 1), providing the opportunity of reacting with CO_2 as the VA-based ECC was cured in air. This phenomenon is consistent with the previous study [28], where dolomite is found in carbonated VA concrete and does not appear in noncarbonated

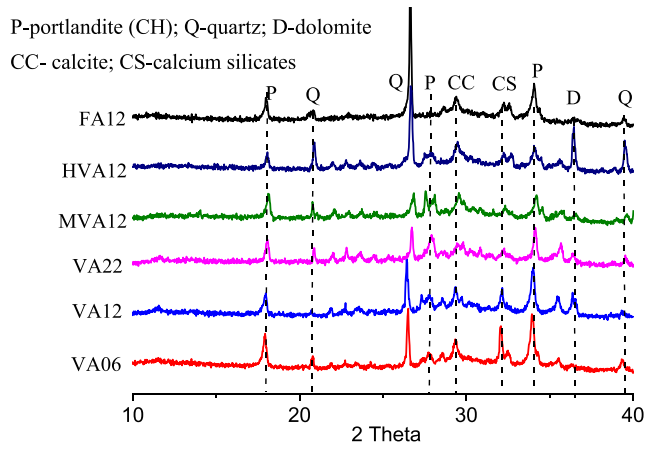

Fig. 15. XRD patterns of the VA-based and FA-based ECC.

VA concrete. Similar mineral products have also been reported in previous VA concrete studies [21,49].

The intensity of portlandite peaks reduced with the increase of the VA/OPC ratio (from 0.6 to 2.2). Also, the CS peaks became less pronounced with the increased levels of the VA/OPC ratio. These observations can be explained by the OPC content in the compositions. V6 has a higher volume of OPC in the mixture than V12 and V22, resulting in more CH products and more residual unhydrated CS as the air-cured samples do not have sufficient water for hydration. The presence of unhydrated CS also indicates a long-term strength gain potential of VA-ECC. The intensity of quartz peaks shows slightly more pronounced in MVA and HVA due to the addition of silica fume (nano-silica). Besides, MVA and HVA have identical mineral product types compared to VA06, VA12, and VA22.

3.4.3. Thermogravimetric analysis

Mass loss of ECC paste from 20 to 950 °C was investigated using the TGA method. Mainly three stages were observed on derivative thermogravimetry (DTG) curves (Fig. 16). The first mass loss occurred at 20–200 °C, accompanied by an exothermic peak at about 120–135 °C depending on ECC compositions, which was attributed to the non-evaporable water bound in hydration products, such as C–S–H [58]. The second mass loss at 300–500 °C with an exothermic peak at about 420 °C was mainly due to dehydroxylation, which was often associated with the decomposition of calcium hydroxide [59]. An exothermic peak appearing between 500 and 850 °C is attributed to the decarbonization of $CaCO_3$.

CH in the hydration product relates to the underlying mechanism of strength development and self-healing capacity. CH is firstly produced by hydration of OPC, then can be consumed by pozzolanic reaction (VA, FA, or SF) and carbonation reaction. Therefore, two temperature ranges of 300–500 °C and 500–850 °C are tabulated in Table 7, corresponding

Table 7
Normalized mass loss of ECC mortars without fibers corresponding to portlandite and calcite decomposition.

Temperature	300-500 (°C)		500-850 (°C)	
Mix. ID	Mass loss (%)	CH (%)	Mass loss (%)	CC (%)
FA12	3.0	12.3	2.7	6.2
VA06	4.1	17.0	4.1	9.3
VA12	3.5	14.6	3.6	8.3
VA22	2.8	11.5	3.2	7.3
MVA12	2.5	10.4	3.5	7.9
HVA12	2.3	9.3	2.8	6.3

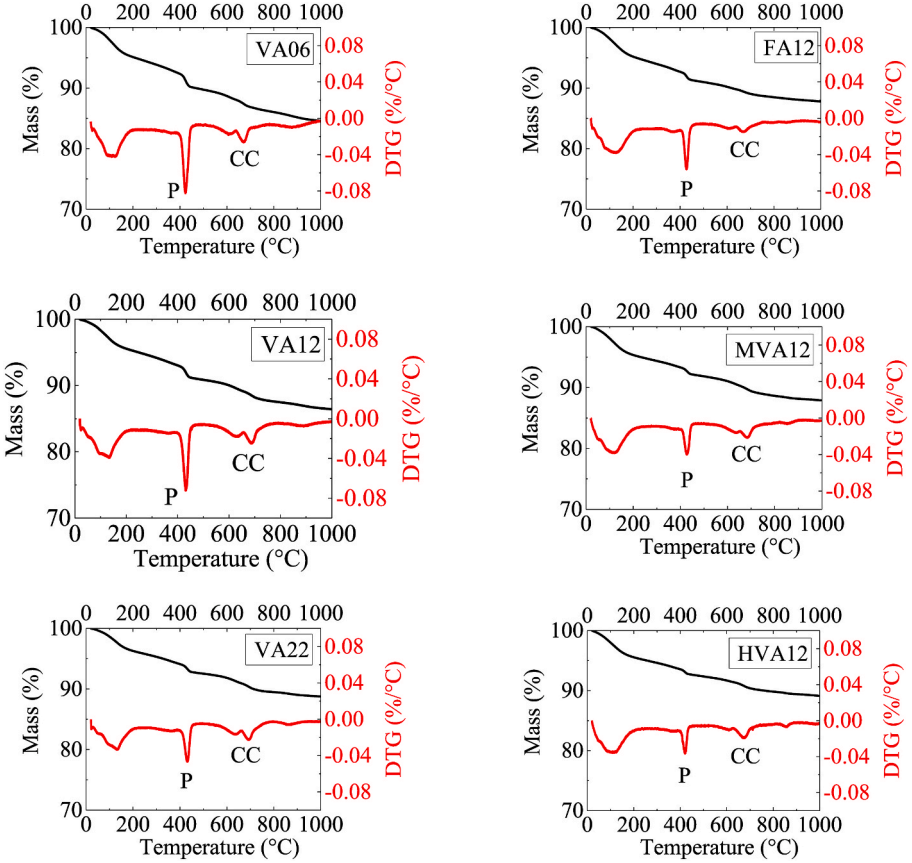

Fig. 16. TGA and DTG of ECC samples without fibers.

to the CH and $CaCO_3$ (CC) amount which may contain carbonation reaction.

Regarding the remaining CH (300–500 °C) after pozzolanic and carbonated reaction, monotonically decreasing intensities were found in VA06, VA12, and VA22 due to their decreasing OPC dosages in compositions. Meanwhile, VA 12 had a higher CH amount (14.6%) than that FA12 (12.3%) reflecting the lower pozzolanic reaction in VA12. The inclusion of SF further decreased the CH amount by MVA12 and HVA12 due to the small particle size and highly reactive silica fume that consumes the CH.

Similar to the CH amount, VA12 had a higher CC content than FA 12 and MVA12. The CC is mainly produced from two sources, the limestone original in OPC, and partial carbonation of CH during curing and sample preparations. Because the OPC volume is identical in FA12, VA12, and MVA12, the difference of CC is mainly caused by the carbonation of CH, suggesting higher carbonation of CH in VA12 than in FA12. Hence, total CH in VA12 should be higher than that of FA12, suggesting that fly ash possesses a higher pozzolanic activity than volcanic ash to consume CH.

The higher pozzolanic activity contributes to the higher strength development of FA12 relative to VA12. In addition, the summed contents of oxide CaO, Al_2O_3, and SiO_2 indicate VA has a lower chemical activity than FA, accounting for the lower strength of VA ECC compared to FA ECC. Moreover, although the crack width of VA12 is larger than FA12, VA12 can obtain a comparable self-healing capacity to FA12 due to the presence of more CH reacting with CO_2 for healing.

4. Conclusions

In this research, an durable ECC via complete replacement of fly ash (FA) with volcanic ash (VA) was demonstrated, providing an alternative solution to FA shortage, especially for geographic regions where VA is plentiful. The rheological, mechanical, and micro performance of VA ECC were comprehensively investigated. Moreover, strategies of rheology control, strength restoration, high ductility, and tiny crack were explored and experimentally verified. Mercury intrusion porosimetry (MIP), X-ray diffraction (XRD), and thermogravimetric analyses (TGA) methods were employed to interpret the underlying micro-mechanisms of macro-mechanical performance. Based on the experimental findings, the following conclusions can be drawn:

- Total replacement of FA with VA in ECC composition requires more water reducer for paste liquefaction and results in severe segregation due to the low viscosity, which can be restored by the addition of hydroxypropyl methylcellulose (HPMC). A minimum viscosity of 6 Pa s was found suitable for PE fibers dispersion. The target viscosity could be engineered by a deliberate combination of HPMC and water reducer. The yield stress of VA-based paste is significantly lower than FA-based paste, suggesting a preference for cast application as opposed to other processes (such as 3D printing) requiring a stiffer paste.
- VA ECC exhibits a 30–40% reduction of compressive strength compared to FA ECC due to the larger particle size, higher porosity, and reduced pozzolanic activity, experimentally verified by MIP and TGA results. The incorporation of silica fume (SF) in the VA-based ECC increases the strength by approximately 15%. Reducing the water/binder ratio from 0.25 to 0.2 in addition to the use of SF results in a compressive strength comparable to FA-based ECC, i.e. 43.8–50.4 MPa depending on the VA to OPC ratio.
- Although VA ECC shows a significant reduction on compressive strength to FA ECC, the VA22 ECC (volcanic ash/OPC = 2.2) has 5.6 MPa of ultimate tensile strength, which is higher than that of FA22 ECC. Moreover, the ductility of volcanic ash ECC is higher than fly ash ECC. The incorporation of silica fume in volcanic ash ECC (MVA ECC) leads to improvements in both tensile strength and ductility. Reducing the water/binder ratio from 0.25 to 0.2 in addition to the use of SF results in a tensile strength of 8.6 MPa and a tensile strain capacity of 12.5%, much higher than the FA ECC in this study.
- Increasing the VA/OPC ratio from 0.6 to 1.2 has insignificant influences on compressive strength, tensile strength, and ductility. Further increase of VA/OPC ratio from 1.2 to 2.4 results in a reduction of strength (compression and tension). However, the tensile ductility is enhanced.
- Crack width follows the lognormal distribution in all mixtures at different strain levels. VA ECC has an average crack width of 50–60 μm, slightly larger than that of FA ECC (40–50 μm). The average crack width generally decreases with the increase of VA volume. The incorporation of silica fume has little influence on the crack width while reducing the water/binder ratio increases the crack width significantly.
- Although VA ECC possesses a slightly larger crack width than FA ECC, VA ECC demonstrates comparable self-healing capacity to FA ECC due to a higher calcium hydroxide content in the VA ECC hydration products, which increases the opportunity for $CaCO_3$ precipitation. The crack recovery ratio depends significantly on the initial crack width, classified as almost fully healed (below 20 μm), partially healed (20–50 μm), and negligibly healed (>50 μm). Beyond crack sealing, ultimate tensile strength is enhanced after wet-dry curing while maintaining a tensile ductility of more than 6%.

The ultra-high ductility (7.4%), tiny crack width (50 μm at failure), and robust self-healing ability of the volcanic ash ECC represent a low-cost and durable ECC using local constituents. These characteristics hold promise in applications in new construction and in rehabilitating aging infrastructures in regions where volcanic ash is plentiful. The proposed rheology engineering method and viscosity control criterion can be generalized for ECC processing with different constituents, such as recycled fine powders, different types of fly ash, rice husk ash, etc. Given the above findings, more investigations on the durability performance of volcanic ash ECC are warranted.

Declaration of competing interest

The authors declare that they have no known competing financial interests or personal relationships that could have appeared to influence the work reported in this paper.

Data availability

Data will be made available on request.

Acknowledgments

This research is supported by a research grant (Contract SATC 2020–004) from Saudi Aramco Technologies Company to the University of Michigan. The authors acknowledge the materials supply from BASF Chemicals Company (water reducer) and Elkem (silica fume).

References

[1] H. Zhu, Y. Hu, Q. Li, R. Ma, Restrained cracking failure behavior of concrete due to temperature and shrinkage, Construct. Build. Mater. 244 (2020), https://doi.org/10.1016/j.conbuildmat.2020.118318.
[2] H. Zhu, Y. Hu, R. Ma, J. Wang, Q. Li, Concrete thermal failure criteria , test method , and mechanism : a review, Construct. Build. Mater. 283 (2021), 122762, https://doi.org/10.1016/j.conbuildmat.2021.122762.
[3] V.C. Li, Engineered Cementitious Composites (ECC), Springer, 2019, https://doi.org/10.1007/978-3-662-58438-5.
[4] E. Cuenca, M. Criado, M. Giménez, M.C. Alonso, L. Ferrara, Effects of alumina nanofibers and cellulose nanocrystals on durability and self-healing capacity of ultrahigh-performance fiber-reinforced concretes, J. Mater. Civ. Eng. 34 (2022) 1–17, https://doi.org/10.1061/(asce)mt.1943-5533.0004375.
[5] E. Cuenca, Autogenous self-healing capacity of early-age ultra-high-performance fiber-reinforced concrete, Sustain. Times 13 (2021) 6–12, https://doi.org/10.3390/su13063061.

[6] E. Cuenca, F. Lo Monte, M. Moro, A. Schiona, L. Ferrara, Effects of autogenous and stimulated self-healing on durability and mechanical performance of uhpfrc: validation of tailored test method through multi-performance healing-induced recovery indices, Sustain. Times 13 (2021), https://doi.org/10.3390/su132011386.

[7] V.C. Li, E.-H. Yang, Self healing in concrete materials, in: Self Heal. Mater., Springer, 2007, pp. 161–193.

[8] H. Liu, Q. Zhang, V. Li, H. Su, C. Gu, Durability study on engineered cementitious composites (ECC) under sulfate and chloride environment, Construct. Build. Mater. 133 (2017) 171–181, https://doi.org/10.1016/j.conbuildmat.2016.12.074.

[9] H. Zhu, D. Zhang, V.C. Li, Centrifugally sprayed engineered cementitious composites: rheology, mechanics, and structural retrofit for concrete pipes, Cem. Concr. Compos. 129 (2022), 104473, https://doi.org/10.1016/j.cemconcomp.2022.104473.

[10] H. Zhu, T. Wang, Y. Wang, V.C. Li, Trenchless rehabilitation for concrete pipelines of water infrastructure: a review from the structural perspective, Cem. Concr. Compos. 123 (2021), 104193, https://doi.org/10.1016/j.cemconcomp.2021.104193.

[11] M.D. Lepech, V.C. Li, R.E. Robertson, G.A. Keoleian, Design of green engineered cementitious composites for improved sustainability, ACI Mater. J. 105 (2008) 567–575, https://doi.org/10.14359/20198.

[12] H. Zhu, D. Zhang, Y. Wang, T. Wang, V.C. Li, Development of self-stressing engineered cementitious composites (ECC), Cem. Concr. Compos. 118 (2021), 103936, https://doi.org/10.1016/j.cemconcomp.2021.103936.

[13] H. Zhu, D. Zhang, T. Wang, H. Wu, V.C. Li, Mechanical and self-healing behavior of low carbon engineered cementitious composites reinforced with PP-fibers, Construct. Build. Mater. 259 (2020), 119805, https://doi.org/10.1016/j.conbuildmat.2020.119805.

[14] X. Huang, R. Ranade, W. Ni, V.C. Li, Development of green engineered cementitious composites using iron ore tailings as aggregates, Construct. Build. Mater. 44 (2013) 757–764, https://doi.org/10.1016/j.conbuildmat.2013.03.088.

[15] Z. Zhang, F. Yang, J.C. Liu, S. Wang, Eco-friendly high strength, high ductility engineered cementitious composites (ECC) with substitution of fly ash by rice husk ash, Cement Concr. Res. 137 (2020), 106200, https://doi.org/10.1016/j.cemconres.2020.106200.

[16] K.Q. Yu, W.J. Zhu, Y. Ding, Z.D. Lu, J. tao Yu, J.Z. Xiao, Micro-structural and mechanical properties of ultra-high performance engineered cementitious composites (UHP-ECC) incorporation of recycled fine powder (RFP), Cem, Concr. Res. 124 (2019), 105813, https://doi.org/10.1016/j.cemconres.2019.105813.

[17] R.P. Borg, E. Cuenca, R. Garofalo, F. Schillani, M.L. Nasner, L. Ferrara, Performance assessment of ultra-high durability concrete produced from recycled ultra-high durability concrete, Front. Built Environ. 7 (2021) 1–20, https://doi.org/10.3389/fbuil.2021.648220.

[18] E. Ghafari, D. Feys, K. Khayat, Feasibility of using natural SCMs in concrete for infrastructure applications, Construct. Build. Mater. 127 (2016) 724–732, https://doi.org/10.1016/J.CONBUILDMAT.2016.10.070.

[19] G. Cai, T. Noguchi, H. Degée, J. Zhao, R. Kitagaki, Volcano-related materials in concretes: a comprehensive review, Environ. Sci. Pollut. Res. 23 (2016) 7220–7243, https://doi.org/10.1007/s11356-016-6161-z.

[20] T.M. Wilson, C. Stewart, V. Sword-Daniels, G.S. Leonard, D.M. Johnston, J.W. Cole, J. Wardman, G. Wilson, S.T. Barnard, Volcanic ash impacts on critical infrastructure, Phys. Chem. Earth (2012) 45–46, https://doi.org/10.1016/j.pce.2011.06.006, 5–23.

[21] K.M.A. Hossain, M. Lachemi, Strength, durability and micro-structural aspects of high performance volcanic ash concrete, Cement Concr. Res. 37 (2007) 759–766, https://doi.org/10.1016/j.cemconres.2007.02.014.

[22] K. Kupwade-Patil, S.H. Chin, M.L. Johnston, J. Maragh, A. Masic, O. Büyüköztürk, Particle size effect of volcanic ash towards developing engineered Portland cements, J. Mater. Civ. Eng. 30 (2018), 4018190, https://doi.org/10.1061/(asce)mt.1943-5533.0002348.

[23] R. Siddique, Properties of concrete made with volcanic ash, Resour. Conserv. Recycl. 66 (2012) 40–44, https://doi.org/10.1016/j.resconrec.2012.06.010.

[24] A.M. Zeyad, A.H. Khan, B.A. Tayeh, Durability and strength characteristics of high-strength concrete incorporated with volcanic pumice powder and polypropylene fibers, J. Mater. Res. Technol. 9 (2020) 806–818, https://doi.org/10.1016/J.JMRT.2019.11.021.

[25] A.M. Zeyad, A. Almalki, Role of particle size of natural pozzolanic materials of volcanic pumice: flow properties, strength, and permeability, Arabian J. Geosci. 14 (2021), https://doi.org/10.1007/s12517-020-06443-y.

[26] S. Al-Fadala, J. Chakkamalayath, S. Al-Bahar, A. Al-Aibani, S. Ahmed, Significance of performance based specifications in the qualification and characterization of blended cement using volcanic ash, Construct. Build. Mater. 144 (2017) 532–540, https://doi.org/10.1016/J.CONBUILDMAT.2017.03.180.

[27] S. Al-Bahar, J. Chakkamalayath, A. Joseph, M. Abdulsalam, S. Al-Otaibi, A. Al-Aibani, Effect of volcanic ash incorporation on the mechanical properties and surface morphology of hydrated cement paste, J. Mater. Civ. Eng. 29 (2017), 4017052, https://doi.org/10.1061/(asce)mt.1943-5533.0001886.

[28] J.H. Seo, I.T. Amr, S.M. Park, R.A. Bamagain, B.A. Fadhel, G.M. Kim, A.S. Hunaidy, H.K. Lee, CO2 uptake of carbonation-cured cement blended with ground volcanic ash, Materials 11 (2018), https://doi.org/10.3390/ma11112187.

[29] K.M.A. Hossain, M. Lachemi, Performance of volcanic ash and pumice based blended cement concrete in mixed sulfate environment, Cement Concr. Res. 36 (2006) 1123–1133, https://doi.org/10.1016/j.cemconres.2006.03.010.

[30] N. Kabay, M.M. Tufekci, A.B. Kizilkanat, D. Oktay, Properties of concrete with pumice powder and fly ash as cement replacement materials, Construct. Build. Mater. 85 (2015) 1–8, https://doi.org/10.1016/J.CONBUILDMAT.2015.03.026.

[31] E. Güneyisi, M. Gesoğlu, S. Al-Rawi, K. Mermerdaş, Effect of volcanic pumice powder on the fresh properties of self-compacting concretes with and without silica fume, Mater. Struct. Constr. 47 (2014) 1857–1865, https://doi.org/10.1617/s11527-013-0155-9.

[32] J. Distlehorst, A. Jenkins, K.D. of Transportation, F.H. Administration, Laboratory Investigation of the Use of Volcanic Ash in Concrete, 2016, p. 58p. http://dmsweb.ksdot.org/AppNetProd/docpop/docpop.aspx?clienttype=html&docid=9671300%0Ahttps://trid.trb.org/view/1423513.

[33] M. Li, V.C. Li, Rheology, fiber dispersion, and robust properties of engineered cementitious composites, Mater. Struct. Constr. 46 (2013) 405–420, https://doi.org/10.1617/s11527-012-9909-z.

[34] H. Zhu, K. Yu, V.C. Li, Sprayable engineered cementitious composites (ECC) using calcined clay limestone cement (LC3) and PP fiber, Cem. Concr. Compos. 115 (2021), 103868, https://doi.org/10.1016/j.cemconcomp.2020.103868.

[35] H. Zhu, K. Yu, V.C. Li, Citric acid influence on sprayable CSA-ECC fresh/hardened properties, ACI Mater. J. 118 (2021) 39–48, https://doi.org/10.14359/51733103.

[36] K. Yu, H. Zhu, M. Hou, V.C. Li, Self-healing of PE-fiber reinforced lightweight high-strength engineered cementitious composite, Cem. Concr. Compos. 123 (2021), 104209, https://doi.org/10.1016/j.cemconcomp.2021.104209.

[37] ASTM C1437-15, Standard Test Method for Flow of Hydraulic Cement Mortar, ASTM International, West Conshohocken, PA, 2015, www.astm.org (n.d.).

[38] D. Feys, J.E. Wallevik, A. Yahia, K.H. Khayat, O.H. Wallevik, Extension of the Reiner-Riwlin equation to determine modified Bingham parameters measured in coaxial cylinders rheometers, Mater. Struct. Constr. 46 (2013) 289–311, https://doi.org/10.1617/s11527-012-9902-6.

[39] M. Nodehi, T. Ozbakkaloglu, A. Gholampour, A systematic review of bacteria-based self-healing concrete: biomineralization, mechanical, and durability properties, J. Build. Eng. 49 (2022), 104038, https://doi.org/10.1016/j.jobe.2022.104038.

[40] E. Tsampali, M. Stefanidou, The role of crystalline admixtures in the long-term healing process of fiber-reinforced cementitious composites (FRCC), J. Build. Eng. 60 (2022), 105164, https://doi.org/10.1016/j.jobe.2022.105164.

[41] D. Zhang, B. Jaworska, H. Zhu, K. Dahlquist, V.C. Li, Engineered Cementitious Composites (ECC) with limestone calcined clay cement (LC3), Cem. Concr. Compos. 114 (2020), 103766, https://doi.org/10.1016/j.cemconcomp.2020.103766.

[42] J. Zhang, G.W. Scherer, Comparison of methods for arresting hydration of cement, Cement Concr. Res. 41 (2011) 1024–1036, https://doi.org/10.1016/j.cemconres.2011.06.003.

[43] Y. Li, X. Guan, C. Zhang, T. Liu, Development of high-strength and high-ductility ECC with saturated multiple cracking based on the flaw effect of coarse river sand, J. Mater. Civ. Eng. 32 (2020), 4020317, https://doi.org/10.1061/(asce)mt.1943-5533.0003405.

[44] C. Gallé, Effect of drying on cement-based materials pore structure as identified by mercury intrusion porosimetry - a comparative study between oven-, vacuum-, and freeze-drying, Cement Concr. Res. 31 (2001) 1467–1477, https://doi.org/10.1016/S0008-8846(01)00594-4.

[45] B. Felekoglu, K. Tosun-Felekoglu, R. Ranade, Q. Zhang, V.C. Li, Influence of matrix flowability, fiber mixing procedure, and curing conditions on the mechanical performance of HTPP-ECC, Compos. B Eng. 60 (2014) 359–370, https://doi.org/10.1016/J.COMPOSITESB.2013.12.076.

[46] K.H. Khayat, Z. Guizani, Use of viscosity-modifying admixture to enhance stability of fluid concrete, ACI Mater. J. 94 (1997) 332–340, https://doi.org/10.14359/317.

[47] E.H. Yang, M. Sahmaran, Y. Yang, V.C. Li, Rheological control in production of engineered cementitious composites, ACI Mater. J. 106 (2009) 357–366, https://doi.org/10.14359/56656.

[48] S. Seraj, R. Cano, R.D. Ferron, M.C.G. Juenger, The role of particle size on the performance of pumice as a supplementary cementitious material, Cem. Concr. Compos. 80 (2017) 135–142, https://doi.org/10.1016/J.CEMCONCOMP.2017.03.009.

[49] G. Yildirim, B. Dündar, B. Alam, I.Ö. Yaman, M. Şahmaran, Role of nanosilica on the early-age performance of natural pozzolan-based blended cement, ACI Mater. J. 115 (2018) 969–980, https://doi.org/10.14359/51706848.

[50] H. Zhu, K. Yu, W. McGee, T.Y. Ng, V.C. Li, Limestone calcined clay cement for three-dimensional-printed engineered cementitious composites, ACI Mater. J. 118 (2021) 111–122, https://doi.org/10.14359/51733109.

[51] H. Liu, Q. Zhang, C. Gu, H. Su, V.C. Li, Influence of micro-cracking on the permeability of engineered cementitious composites, Cem. Concr. Compos. 72 (2016) 104–113, https://doi.org/10.1016/j.cemconcomp.2016.05.016.

[52] R. Ranade, J. Zhang, J.P. Lynch, V.C. Li, Influence of micro-cracking on the composite resistivity of engineered cementitious composites, Cement Concr. Res. 58 (2014) 1–12, https://doi.org/10.1016/j.cemconres.2014.01.002.

[53] H. Ma, E. Herbert, M. Ohno, V.C. Li, Scale-linking model of self-healing and stiffness recovery in Engineered Cementitious Composites (ECC), Cem. Concr. Compos. 95 (2019) 1–9, https://doi.org/10.1016/J.CEMCONCOMP.2018.10.006.

[54] L.L. Kan, H.S. Shi, A.R. Sakulich, V.C. Li, Self-healing characterization of engineered cementitious composite materials, ACI Mater. J. 107 (2010) 617–624, https://doi.org/10.14359/51664049.

[55] Z. Zhang, Q. Zhang, Self-healing ability of Engineered Cementitious Composites (ECC) under different exposure environments, Construct. Build. Mater. 156 (2017) 142–151, https://doi.org/10.1016/J.CONBUILDMAT.2017.08.166.

[56] M. Wu, B. Johannesson, M. Geiker, A review: self-healing in cementitious materials and engineered cementitious composite as a self-healing material, Construct. Build. Mater. 28 (2012) 571–583, https://doi.org/10.1016/j.conbuildmat.2011.08.086.

[57] C. Zhang, X. Guan, J. Li, Y. Li, R. Lu, Coupling effect of cementitious capillary crystalline waterproof material and exposure environments on self-healing

properties of engineered cementitious composites (ECC), J. Build. Eng. 63 (2023), 105471, https://doi.org/10.1016/j.jobe.2022.105471.
[58] Ž. Sekulić, S. Popov, M. Uričić, A. Rosić, Mechanical activation of cement with addition of fly ash, Mater. Lett. 39 (1999) 115–121, https://doi.org/10.1016/S0167-577X(98)00226-2.
[59] D. Zhang, X. Cai, B. Jaworska, Effect of pre-carbonation hydration on long-term hydration of carbonation-cured cement-based materials, Construct. Build. Mater. 231 (2020), 117122, https://doi.org/10.1016/j.conbuildmat.2019.117122.